REPORT DOCUMENTATION PAGE

READ INSTRUCTIONS BEFORE COMPLETING FORM

1. REPORT NUMBER: NORDA Report 64	2. GOVT ACCESSION NO.
3. RECIPIENT'S CATALOG NUMBER	
4. TITLE (and Subtitle): Comments and Issues Pertinent to SHARPS III Near-Surface Propagation Modeling	5. TYPE OF REPORT & PERIOD COVERED: Final
6. PERFORMING ORG. REPORT NUMBER	
7. AUTHOR(s): Robert W. McGirr	8. CONTRACT OR GRANT NUMBER(s)
9. PERFORMING ORGANIZATION NAME AND ADDRESS: Naval Ocean Research & Development Activity, Ocean Acoustics & Technology Directorate, NSTL, Mississippi 39529	10. PROGRAM ELEMENT, PROJECT, TASK AREA & WORK UNIT NUMBERS: 63785N
11. CONTROLLING OFFICE NAME AND ADDRESS: Same	12. REPORT DATE: October 1983
	13. NUMBER OF PAGES: 34
14. MONITORING AGENCY NAME & ADDRESS (if different from Controlling Office)	15. SECURITY CLASS. (of this report): UNCLASSIFIED
	15a. DECLASSIFICATION/DOWNGRADING SCHEDULE

16. DISTRIBUTION STATEMENT (of this Report)

Approved for Public Release
Distribution Unlimited

17. DISTRIBUTION STATEMENT (of the abstract entered in Block 20, if different from Report)

18. SUPPLEMENTARY NOTES

19. KEY WORDS (Continue on reverse side if necessary and identify by block number)

underwater acoustics
propagation loss
prediction models
surface ducts

20. ABSTRACT (Continue on reverse side if necessary and identify by block number)

The propagation submodels of SHARPS-III are assessed for their applicability to near-surface sound velocity conditions. The near-surface channel configurations addressed by the current version of SHARPS are too limited. The options are limited to surface ducts and subsurface ducts, as modeled by the Advanced AMOS equations. All other channel configurations are handled by ray theory. A SHARPS input known as the sonic layer depth (SLD) is demonstrated to be in occasional contrast with the layer depth of a classical surface duct. Simple
(continued)

expressions based on ray theory and phase integral methods are used to demonstrate the sensitivity of selected acoustic parameters to variations of in-layer sound velocity gradient. Changes that have been made to the original AMOS equations are reviewed. The depth dependence of a gradient-sensitized version of AMOS is analyzed. Some long-standing near-surface propagation issues are reviewed, and results from a recent evaluation of several operational surface duct models are represented.

NORDA Report 64

Comments and Issues Pertinent to SHARPS III Near-Surface Propagation Modeling

R. W. McGirr

Numerical Modeling Division
Ocean Science and Technology Laboratory

October 1983

Naval Ocean Research and Development Activity
NSTL, Mississippi 39529

Foreword

The Tactical ASW Environmental Acoustic Support program office has been chartered to maintain and upgrade prediction models that are in operational use at the Fleet Numerical Oceanography Center, Monterey. This report presents an assessment of the near-surface propagation submodels currently used in SHARPS III.

G.T. Phelps, Captain, USN
Commanding Officer, NORDA

Executive Summary

The propagation submodels of SHARPS III are assessed for their applicability to near-surface sound velocity conditions. The near-surface channel configurations addressed by the current version of SHARPS are too limited. The options are limited to surface ducts and subsurface ducts, as modeled by the Advanced AMOS equations. All other channel configurations are handled by ray theory. A SHARPS input known as the sonic layer depth (SLD) is demonstrated to be in occasional contrast with the layer depth of a classical surface duct. Simple expressions based on ray theory and phase integral methods are used to demonstrate the sensitivity of selected acoustic parameters to variations of in-layer sound velocity gradient. Changes that have been made to the original AMOS equations are reviewed, and results from a recent evaluation of several operational surface duct models are presented.

Acknowledgments

The author wishes to express his appreciation to D. White and Dr. D. B. King for their technical review and helpful suggestions, and to W. W. Renner and W. D. Kirby of Science Applications, Inc., for making data available from their evaluation of sound velocity profile filters.

The work reported here was conducted under program element 63785N and project number R0120SH. The sponsoring activity was the Tactical ASW Environmental Acoustic Support program office, E. D. Chaika, Program Manager.

Contents

Illustrations

Comments and Issues Pertinent to SHARPS III Near-Surface Propagation Modeling

1.0 Introduction

This report addresses near-surface propagation modeling issues pertinent to the Ship Helicoptor Active Range Prediction System (SHARPS). SHARPS is implemented on a daily basis to generate forecasts of detection range for Fleet active sonar systems operating in a wide variety of ocean environments. The schedule and volume of forecasts and requests preclude the use of highly sophisticated acoustic models. Consequently, specific modules of SHARPS are required to satisfy stringent computation time specifications.

In an effort to meet these specifications a semiempirical model derived from the AMOS data (Marsh and Schulkin, 1954) has provided the basis for near-surface propagation modeling in both the second and third generation versions of SHARPS. The basic AMOS model accommodates two modes of propagation: surface duct and subsurface duct. The intention here is to shed some light on problems noted with SHARPS detection range forecasts with the focus centering on those problems thought to be caused by the surface duct component of the modified AMOS model. The position taken here is that the AMOS model, with or without modifications, does a decent job for near-surface sound velocity conditions that are appropriate. Therein lies the problem: near-surface conditions are not always appropriate for the application of AMOS. Indeed, conditions can exist such that even fairly sophisticated normal mode models do not, on average, yield "better" prediction than AMOS (Hall, 1980).

The report consists of three major sections:

- Section 2 addresses the distinction between layer depth (for a surface duct) and a SHARPS input known as the sonic layer depth (SLD). Predominant profile configurations gleaned from the SUDS I experiment are also presented as a summary of channel configurations that need to be addressed by near-surface propagation models. Simple expressions based on ray theory and phase integral methods are used to demonstrate the sensitivity of selected acoustic parameters to variations of in-layer sound velocity gradient.

- Section 3 reviews the changes that have been made to the original version of AMOS. The depth dependence of a gradient-sensitized version of AMOS is analyzed.

- Section 4 reviews some long-standing near-surface propagation issues and presents results from a recent evaluation of several operational surface duct models. The report closes with a section that presents conclusions and recommendations.

2.0 Near-Surface Sound Velocity Conditions

This section examines near-surface sound velocity conditions, with emphasis on the classical surface duct configuration. The question providing much of the impetus for such an examination is:

> are two-layer surface duct models adequate for modeling the propagation conditions under which active sonars echo range against snorkeling or deep-running boats?

The discussion begins with a definition of "layer depth." Some statistics derived from Surface Duct Sonar (SUDS) I

data are used as guidelines in a discussion of important channel configurations. The last subsection exploits two simple approaches to demonstrate the sensitivity of various acoustic parameters to in-layer velocity gradient.

2.1 The Layer Depth Problem

In the upper few hundred meters of the water column, processes involving water mixing and a net heat flow toward the surface can develop a thermal structure that produces a surface duct. This condition is characterized by a nearly constant (isothermal) or slightly increasing water temperature extending from the surface down to the depth of significant mixing. Below this depth temperature decreases sharply. The depth interval over which this sharp decrease occurs is referred to as the thermocline. Under these conditions, if salinity is constant, sound velocity increases with depth from the surface to the top of the thermocline (or layer depth), and decreases sharply below this depth. This increasing velocity function above the thermocline creates a near-surface sound channel, referred to as a surface duct. Thus a surface duct is a near-surface sound channel that consists of a half-channel (with axis at the surface) setting on top of the thermocline. The depth at which the half-channel meets the thermocline is the layer depth.

This last point is to be emphasized since the term layer depth, as used here, is restricted to a channel configuration known as the classical bilinear surface duct. A similar term, sonic layer depth (SLD), is routinely used at FNOC, and this term does not necessarily coincide with the one described above. Indeed, after examining velocity profiles produced over a one month period by FNOC, SLD appears to coincide more closely with the top of the thermocline. However, the fact that the thermocline does not extend to the surface does not necessarily imply the existence of a surface duct.

A value of SLD is included in each SHARPS message along with detection range forecasts. Based on criticisms levied against SHARPS forecasts, a non-zero value of SLD is evidently interpreted by some message recipients to mean that a surface duct is present. If a non-zero SLD is assumed to imply that a surface duct exists, and if predicted detection ranges for certain sonar systems do no reflect this assumption, then such forecasts no doubt engender puzzlement at the very least.

Renner and Kirby (1983), in an attempt to solve the SLD problem, assessed the performance of three sound velocity profile filters. The purpose of their analyses was to determine if removing "fine structure" from the upper portion (above the SLD) of the profile input would eliminate the much criticized day-to-day variability observed in SHARPS predicted detection ranges. To evaluate the candidate filters, a data base containing 30 daily samples of FNOC-generated sound velocity profiles for eight ocean areas was assembled.

Included with each profile was the SLD as determined by an algorithm in EXTRAC, a pre-SHARPS profile processing program. Figure 1 illustrates a 30 day sequence of profiles for one of the sites (Note: profiles for days 22 and 27 are missing). The left-to-right sequencing, with a 1 m/sec offset to facilitate visual discrimination, simulates a daily time series. The FNOC-generated profiles are represented by the solid curves and filtered renditions are indicated by the dashed curves. Near the top of each profile there is a short horizontal marker that indicates the reported SLD. This sequence of profiles exhibits extremely scant variation in SLD. Indeed, the change in SLD over a 30 day period amounts to only a few meters. Most of the profiles from day 1 through day 20 exhibit surface ducts. A few are blighted by a slightly negative-gradient layer at the top. The remaining profiles from day 21 through day 30

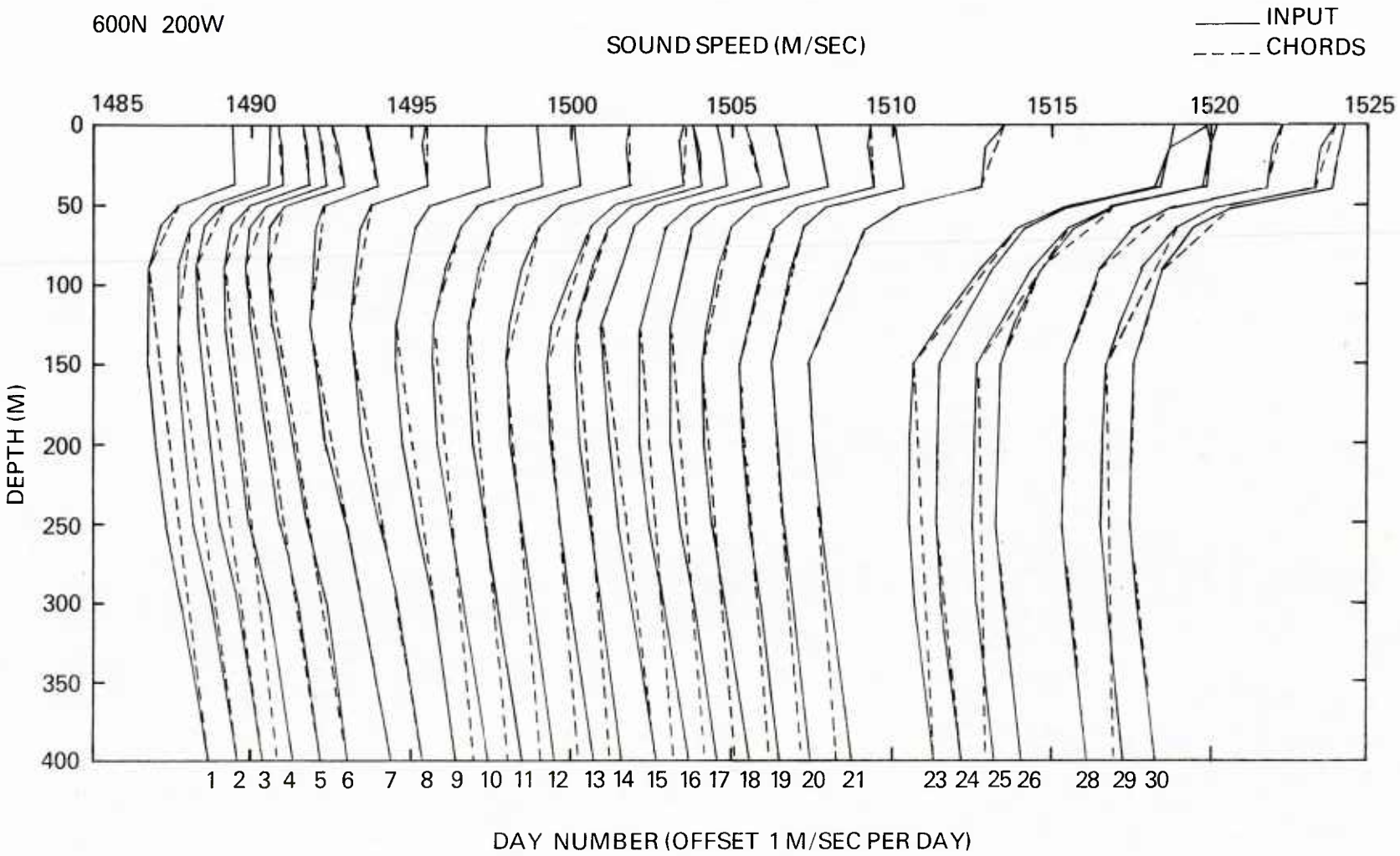

Figure 1. 30-Day sequence of FNOC profiles

do not exhibit surface ducts. All of these profiles, however, have an SLD of about 40 m. Thus SHARPS predictions generated for any of the profiles from this set would indicate an SLD of about 40 m. In some cases there is a surface duct, and in some cases there is a negative gradient. The point is, a non-zero value of SLD does not necessarily imply the existence of a surface duct.

Three modes of near-surface propagation are addressed by SHARPS: negative gradient, surface duct, and subsurface duct. The negative gradient case is calculated by ray theory out to the shadow boundary and by a diffraction continuation term into the shadow zone. Both the surface duct and subsurface duct cases are calculated by the modified AMOS equations. Any of these modes, as well as other possibilities, can be extant for a non-zero SLD. If the velocity gradient between the surface and the SLD is negative, detection ranges for many sonar-target geometries can be expected to be short. When the velocity gradient is positive, detection ranges can exhibit considerable latitude--depending on the "strength" of the channel, as well as other factors that enter into the sonar equation. Consequently, in terms of what detection ranges to expect, a non-zero value of SLD provides no conclusive information.

The reason for including SLD in the SHARPS message needs to be reviewed. Since no other data are included to indicate the profile configuration above the SLD, its inclusion with regard to detection range predictions provides more confusion than information. In those cases when the SLD coincides with the depth of a surface duct, the inclusion of SLD on the message makes sense. Its inclusion might also make sense to a conservative submarine skipper. That is, regardless of the channel configuration above the SLD, a conservative strategy for detection avoidance (by hull mounted sonars), would be to keep the boat below SLD. Otherwise its inclusion is, at best, curious.

One possible approach to rectifying this problem has been suggested by LaDouce (personal communication 1983). Simply put, SLD would continue to be included in the SHARPS message, but if the profile configuration does not conform to a two-layer surface duct, then this decision should somehow be indicated, perhaps on a different line of the message. In this way, the value of SLD as determined by a pre-SHARPS profile processing program is retained on the message, yet its significance (or lack of) with regard to surface duct detection performance is clarified.

Unfortunately, this simple remedy does not solve the problem completely. Figure 2 illustrates an "indeterminant" profile configuration observed by Renner and Kirby (1983) in their analysis of FNOC-generated profiles. The "indeterminancy" stems from the inconsistency of the EXTRAC program in defining

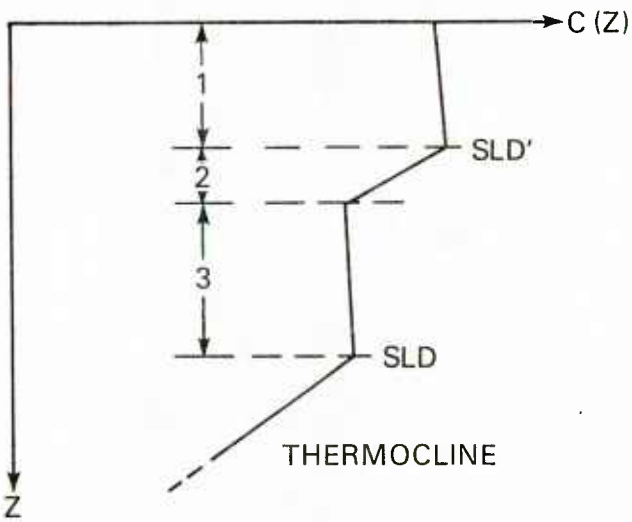

Figure 2. Profile illustrating indeterminant SLD

SLD. For most cases the deeper SLD was selected, corresponding to the top of the thermocline. On occasion, however, whenever the gradient of the second layer was strong enough, the upper SLD was selected. This configuration is comprised of a near-surface half channel overlaying a weak refractive channel overlying the thermocline. Which of the two SLDs indicated on the figure is the "real" one? For geometries where both sonar and target are in the upper layer, a two-layer surface duct model based on channel parameters derived from the first two layers would be appropriate. If the target is located in the third layer, however, then application of a two-layer model poses a problem. The "solution" will probably not make itself evident in the form of a simple two-layer model.

2.2 Important Near-Surface Channel Configurations

One of the revelations derived from the SUDS I experiment is that surface ducts do not necessarily sustain for either long durations or long distances. This unfortunate circumstance has been confirmed by data obtained during subsequent exercises as well. What is more, there appear to be several near-surface profile configurations as important (and some may be even more important) as the classical two-layer surface duct profile.

According to Anderson and Pedersen (1976) the most prevalent profile configuration observed during the SUDS I experiment is that of a surface duct above a subsurface (or depressed) duct. Indeed, this configuration accounts for 34% of the recorded profiles. The classical two-layer surface duct configuration accounts for only 17.6%. Moreover, three other profile configurations were observed nearly as often as the classical surface duct. These configurations are: (1) a positive-gradient layer over two negative-gradient layers, (2) a negative-gradient channel, and (3) a non-symmetric depressed duct (in some cases a surface duct exhibiting the "afternoon" effect). These three configurations account for 16.5%, 15.7%, and 15.1% of the measurements, respectively.

Figure 3 exhibits seven important near-surface velocity profile configurations. Of these, SHARPS can make nonray theory predictions for only two: a surface duct (profile A) and a subsurface duct (profile C). Profile F is the most important profile configuration (according to SUDS I statistics), and can be handled by the AMOS model only under certain restrictions. These restrictions are based on sonar-target geometries. If both sonar and target are located in the upper (positive-gradient) layer then the surface duct equations are applicable. If both sonar and target are located in the depressed channel then the subsurface duct equations are applicable. However, the AMOS model does not provide for cross-channel coupling, and, therefore, other sonar-target goemetries are handled by ray theory.

The profile configuration illustrated in part D exhibits what is commonly referred to as the "afternoon" effect. Its configuration coincides with the

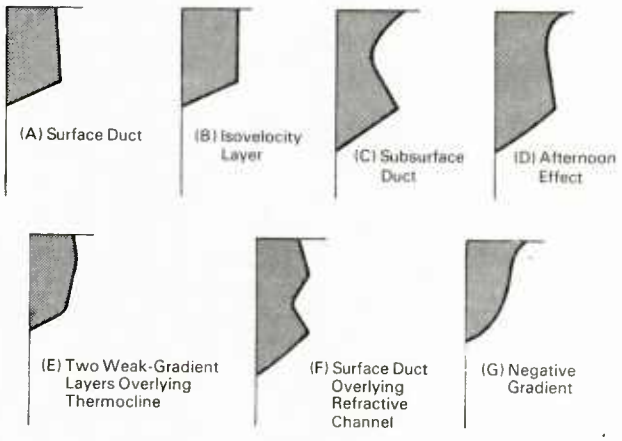

Figure 3. Important near-surface sound velocity profile configurations

classical two-layer surface duct except for the upper few meters where there is a negative gradient. According to Frost (personal communication 1982), this type of profile is not just an afternoon phenomenon, at least in the Mediterranean Sea, but rather it tends to be seasonal. The important point here is that the subsurface duct model of AMOS is not applicable for this case because of the extreme asymmetry exhibited by the majority of such channels.

Other important profile configurations not modeled by SHARPS are illustrated in parts B and E. These configurations appear to be quite similar to the classical surface duct, but some important differences exists with regard to propagation modeling. In profile B, an isovelocity channel, there is a distinct absence of an energy barrier. The AMOS surface duct equations were derived from data which, on average, exhibit the requisite barrier. Thus, simply setting the in-layer gradient to some arbitrarily small lower bound does not necessarily qualify a gradient-sensitized version of AMOS as a decent model for isovelocity channels. A similar remark holds for profile E. This configuration has two weak-gradient layers above the thermocline. An equivalent single-layer gradient could easily, in many instances, be isovelocity or negative. Here again, the AMOS model cannot properly model either of these situations.

The profile configuration shown in part G is handled by ray theory in SHARPS. A ray theory treatment for this channel configuration is perfectly acceptable, especially when a means to continue the solution into the shadow zone is appended, as it is in SHARPS. A criticism of this approach, however, regards the matter of consistency. There is the possibility of a distinct discontinuity of results as the in-layer gradient varies from slightly positive (AMOS) to slightly negative (ray theory).

A point not dwelled upon in this discussion pertains to the matter of profile stability. Many of the SUDS measurement events yielded results in stark constrast to the 30-day FNOC sequence illustrated in Figure 1. That is, instead of a relatively constant SLD characteristic of the FNOC sequence, many of the SUDS events revealed highly variable layer depths over track segments extending over only a few kilometers. To what extent this degree of variability prevails is generally unknown. If unstable near-surface conditions are the rule, then differences observed between SHARPS predictions and actual detection performance are understandable. However, if significant differences are observed in regions known to be fairly stable, then only detailed analyses can resolve the myriad causes for discrepancies.

2.3 Sensitivity of Acoustic Parameters to In-Layer Gradients

This section presents results that demonstrate the sensitivity of selected acoustic parameters to changes in the sound velocity gradient within the upper layer of a classical two-layer surface duct. The impetus is provided by a long-standing complaint casually voiced by SHARPS critics. Essentially the complaint stems from the observation that as the in-layer thermal gradient fluctuates about zero, predicted detection ranges exhibits unexpectedly large fluctuations.

Two simple methods are used to demonstrate sensitivity results. The first method uses ray theory to illustrate the dependence of the channel-limiting cycle-range on gradient. Conclusions that can be drawn regarding active-system detection ranges are shown to be strongly dependent on considerations not necessarily related to the in-layer gradient. The second method uses phase-integral and Wentzel-Kramers-Brillouin (WKB) results to demonstrate how several "mode" parameters vary with gradient.

2.3.1 Cycle-Range Sensitivity

The sensitivity of sonar-to-target range calculations to variations in sound velocity gradient can be demonstrated using a ray invariant. The particular ray invariant selected for this purpose takes the form of the channel-limiting cycle range. An example of a corresponding ray trajectory is depicted in Figure 4.

All cycle-range results presented here are based on a profile model of the form

$$C(Z) = C_o/\sqrt{1 - \beta Z}\ , \quad Z < Z_L \tag{1}$$

where $\beta = 2g/C_o$, and where g and C_o are the in-layer velocity gradient and sound velocity at the surface. With this representation, the index of refraction squared is a linear function of depth. Using this profile model, the range integral can be written in the form

$$r(Z) = \beta^{-1/2}(C_o/C_m)\int_o^Z (Z_m - Z')^{-1/2}\, dZ' \tag{2}$$

or,

$$r(Z) = -2\beta^{-1/2}(C_o/C_m)(Z_m - Z)^{-1/2} + \text{const} \tag{3}$$

where Z_m and C_m are the turning point depth and sound velocity. The channel-limiting cycle range is twice this integral evaluated from the surface to the bottom of the layer, or

$$r_c = 2[r(Z_L) - r(0)]$$

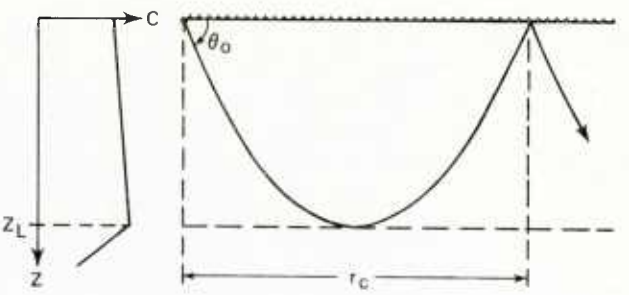

Figure 4. Channel-limiting ray

$$\text{or,}\quad r_c = 4\beta^{-1/2}(C_o/C_L)Z_L^{1/2} \tag{4}$$

where C_L is the sound velocity at the layer depth. Using Snell's law this result may be expressed as

$$r_c = (C_o/g)\sin 2\theta_o \tag{5}$$

where θ_o is the launch angle of the ray trajectory. Figure 5 illustrates curves of channel-limiting cycle range generated by Eq. (5) as a function of in-layer gradient. The sound velocity at the surface is taken to be 5000 fps, and four curves are generated for layer depths of 50, 150, 250, and 350 feet.

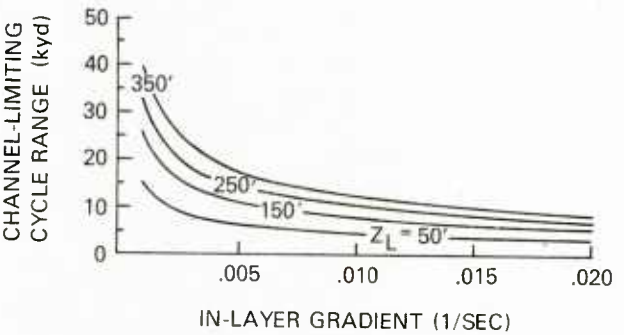

Figure 5. Channel-limiting cycle range versus in-layer gradient

These curves demonstrate that cycle range increases as the in-layer gradient decreases. These results also hold for sonar and target at arbitrary depths within the layer, as long as the range integral is evaluated over a complete cycle.

The implications of these results with regard to detection range are difficult to assess in general. In situations where volume attenuation and surface losses are not overbearing, some indication of the impact on propagation loss can be gleaned from the modified AMOS model (Section 3.2). From Eq. (6) the transition zone between spherical and cylindrical spreading regimes can be seen to extend to ranges somewhat beyond the channel-limiting cycle range. Inside this zone, the nondissipative contribution to propagation loss is generally not too significant. The major increase to propagation loss as this zone extends in range is due to the volume attenuation term, $\alpha_V r$. In this case there is the possibility that detection range increases with decreasing gradient, at least out to that range where the attenuation term causes the propagation loss to exceed a given FOM.

As an example of this possibility, consider the following case. Suppose that a short-pulse sonar is closing on a high-Doppler target, so that reverberation returns are shifted out of the processing band. In such a case the search operation is conducted under noise-limited conditions. As a consequence the sonar equation assumes the simple form

$$SE = SL - 2\,PL + TS - NL - RD, \qquad (6)$$

where SE is signal excess, SL is source level, PL is one-way propagation loss, TS is target strength, NL is noise level, and RD is recognition differential. Let SL = 220 dB, TS = 15 dB, NL = 60 dB, and RD = -5 dB. SE = 0 corresponds to a single-ping detection probability of 0.5, so that

$$2\,PL = 180\ dB$$

yields the value of PL that corresponds to the detection range. For this contrived example, propagation loss monotonically increases with range, and, therefore, finding the detection range is a simple process.

Figure 6 illustrates five one-way propagation loss versus range curves generated by a gradient-sensitive version of AMOS. The five values of in-layer velocity gradient selected for this example are 0.02, 0.01, 0.005, 0.0025, and 0.001 (1/sec). The dashed line represents the equivalent one-way FOM level of 90 dB. The detection ranges are determined by noting where the curves intercept the FOM line. These ranges are indicated on the figure, and can be seen to increase for decreasing gradient. Indeed, the resulting variations in detection range to changes in gradient are consistent with the results presented in Figure 5.

This degree of sensitivity is not always so evident, as the following example demonstrates. Suppose that surface reverberation is dominant, so that the masking level essentially coincides with the surface reverberation level. The sonar equation then takes the form

$$SE = SL - 2PL + TS - RL - RD.$$

The reverberation level, RL, in this case is given by

$$RL = SL - 2PL' + SS + 10 \log A,$$

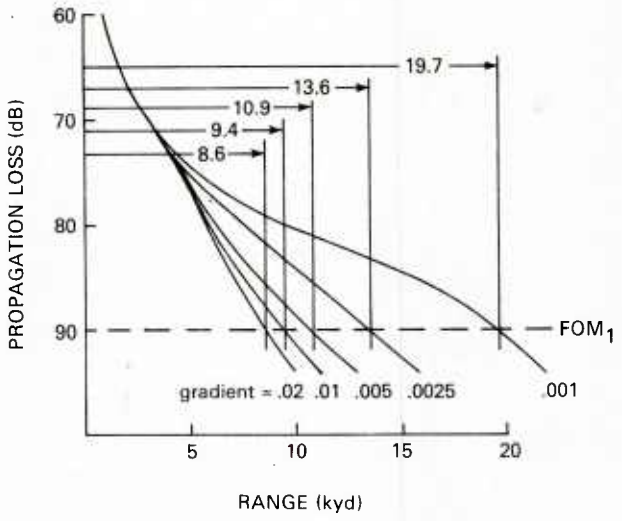

Figure 6. PL vs R curves intercepting FOM level

where SS denotes surface backscattering strength and A is the area of surface ensonified. Thus signal excess may be expressed as

$$SE = 2(PL' - PL) + TS - SS$$

$$- 10 \log A - RD$$

where for simplicity beam pattern corrections have been ignored.

The difference between PL and PL' is not likely to be significant since returns from the surface have to arrive at the same time as the target echoes. Hence the propagation paths (confined to a surface duct) are not radically different. Thus,

$$SE \cong TS - SS - 10 \log A - RD$$

indicating that the detection range is largely dependent on factors other than those involved in propagation.

The analyses employed in these examples are overly simplified, but the intent here is to examine two contrasting possibilities. These two examples indicate that the expected sensitivity of detection range to in-layer gradient is strongly evident under one set of conditions.

Generally, rules of thumb can be fruitfully applied under the right conditions, but more often than not they are belied by the intrinsic complexities of the ocean medium. Sonar system performance prediction, in particular, is confounded by an infrastructure of factors far too complex to accede to simple rules of thumb. The application of simple ray theory, for example, with no consideration given to other factors, can lead to conclusions that do not always converge toward ground truth.

2.3.2 Mode Parameter Sensitivity

This section exploits phase integral and WKB methods to analyze the sensitivity of certain mode parameters to variations of in-layer sound velocity gradient. Derivations for most of the expressions used here are not included, since they are adequately presented by Furry (1945) and by Freehafer (1951). These methods have been applied to underwater acoustic surface duct problems by several investigators over the past two decades. Pedersen and Gordon (1965) make use of these methods to obtain starting eigenvalues required for normal mode solution. Kibblewhite and Denham (1965) exploit these methods to analyze experimental surface duct data. In more recent work, Hall (1976) investigates the accuracy of WKB solutions for the surface duct problem, and Barnard and Deavenport (1978) use the phase integral method to incorporate surface roughness effects into a normal mode solution.

The results used in this sensitivity analysis stem from the phase integral and approximate (WKB) solutions to the reduced wave equation. This equation takes the form

$$d^2u/dz^2 + k_o^2 su = 0 \qquad (7)$$

where $k_o = 2\pi f/C_o$, and

$$s = N(Z)^2 - (k_n/k_o)^2. \qquad (8)$$

N(Z) is the index of refraction, $C_o/C(Z)$, and k_n is the usual separation parameter. If interest is confined to in-layer solutions, the real part of k_n is significantly larger than the imaginary part and useful approximate solutions to Eq. (7) can be obtained by replacing k_n with $K_n = Re(k_n)$. With this stipulation the solutions to Eq. (7) are given by

$$U_n(Z) = A_n s^{-1/4} \cos\Big[k_o \int_Z^{Z_n} s^{1/2}\, dz - \pi/4 \Big], \quad 0 < Z < Zn \qquad (9a)$$

and

$$U_n(Z) = \tfrac{1}{2} A_n |s|^{-1/4} \exp\Big[-k_o \int_{Z_n}^{Z} |s|^{1/2} dz\Big], \quad Z_n < Z < Z_L \qquad (9b)$$

where Z_L denotes layer depth and Z_n is the turning point depth of the n-th mode. The normalization factor, A_n, is

$$A_n = \Big(2/\int_o^{Z_n} s^{-1/2} dz\Big)^{1/2} \qquad (10)$$

The basic form of the phase integral is

$$2\, k_o \int_o^{Z_n} s^{1/2} dz + \phi_u + \phi_L = 2m\pi, \; m=0, 1, \ldots \qquad (11)$$

For an $\exp(-i\omega t)$ time dependence the phase-change terms are $\phi_u = -\pi$ for surface reflections and $\phi_L = -\pi/2$ for partial wave reflections at the turning points, and hence Eq. (11) takes the more specific form

$$2\, k_o \int_o^{Z_n} s^{1/2} dz = 2(m + 3/4)\pi.$$

Dividing out the 2 and replacing m by n-1, where n is the mode index, this result becomes

$$k_o \int_o^{Z_n} s^{1/2} dz = (n - 1/4)\pi, \; n=1, 2, \ldots \qquad (12)$$

Using the profile model given by Eq. (1)

$$|s|^{1/2} = \big[|N(Z)^2 - (K_n/k_o)^2|\big]^{1/2} = \beta^{1/2}(|Z_n - Z|)^{1/2} \qquad (13)$$

where $Z_n = [1 - (K_n/k_o)^2]/\beta$. The K_n are solutions to the characteristic equation $U_n(0) = 0$. From Eq. (9a) this condition is satisfied for K_n such that

$$k_o \int_o^{Z_n} s^{1/2} dz - \pi/4 = m\pi/2,$$

$$m = 1, 3, 5, \ldots \qquad (14)$$

After shifting to the mode index, this condition coincides with Eq. (12). Thus $K_n = 2\pi f/C_n$, C_n being the sound velocity at the turning point depth Z_n. Carrying out the integration indicated in Eq. (12) yields

$$(2k_o/3)\beta^{1/2} Z_n^{3/2} = (n - 1/4)\pi \qquad (15)$$

so that

$$Z_n = [3(n - 1/4)\pi/2\ k_o^{-1}\beta^{-1/2}]^{2/3} \qquad (16)$$

Freehafer (p. 96, 1951) defines the quantity

$$H = (k_o^2\beta)^{-1/3} \qquad (17)$$

which serves as a "natural" unit of depth. In terms of H the expression for Z_n becomes

$$Z_n = [\ 3(n - 1/4)\pi/2]^{2/3} H. \qquad (18)$$

The number of trapped modes is obtained from this equation by setting Z_n equal to the layer depth, or

$$N = 1/4 + (2/3\pi)(Z_L/H)^{3/2} \qquad (19a)$$

or,

$$N = 1/4 + (2/3)\ (2Z_L/C_o)^{3/2}\ fg^{1/2} \qquad (19b)$$

Figure 7 presents curves illustrating how the number of trapped modes varies with in-layer gradient.

The lowest (cutoff) frequency that will allow just one trapped mode is also obtained from Eq. (18) with $Z_n = Z_L$, and is given by

$$f_{co} = 2^{-9/2} 9(C_o/Z_L)^{3/2}/g^{1/2}. \qquad (20a)$$

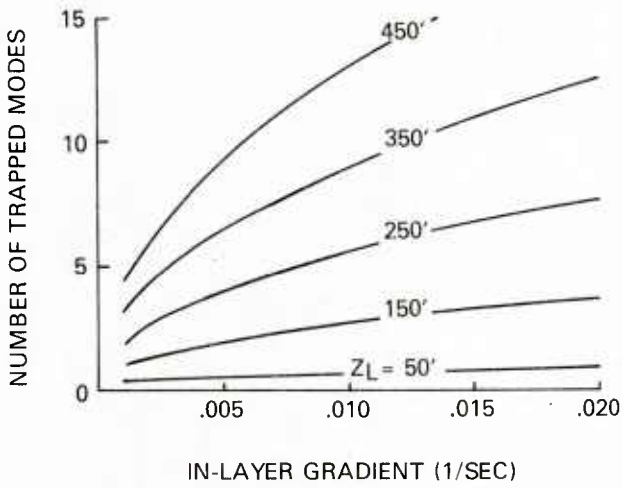

Figure 7. Number of modes versus in-layer gradient

Representing C_o by a nominal value results in some simplification. For C_o = 1500 m/s,

$$f_{co} = 23107(g\ Z_L^3)^{-1/2} \quad (Z_L \text{ in meters}) \tag{20b}$$

and for C = 5000 ft/sec,

$$f_{co} = 140625(g\ Z_L^3)^{-1/2} \quad (Z_L \text{ in feet}) \tag{20c}$$

Figure 8 presents curves illustrating how the mode cutoff frequency varies with in-layer gradient.

Holding everything else constant, the shallowest duct that will support only one trapped mode is obtained from Eq. (18) by setting n = 1, or

$$\min (Z_L) = (9\pi/8)^{2/3} H \cong 2.32\ H$$

or

$$\min (Z_L) = (2\pi^{2/3} C_o f^{2/3} g^{1/3})^{-1}. \tag{21}$$

Figure 9 displays curves illustrating how minimum layer depth varies with in-layer gradient.

Pedersen and Gordon (1965) present a dimensionless parameter, M, that serves as a measure of the "strength" of a surface duct. This parameter is given by

$$M = Z_L/H \tag{22}$$

For conditions near cutoff the number of modes as determined by Eq. (19) is actually a noninteger value that falls

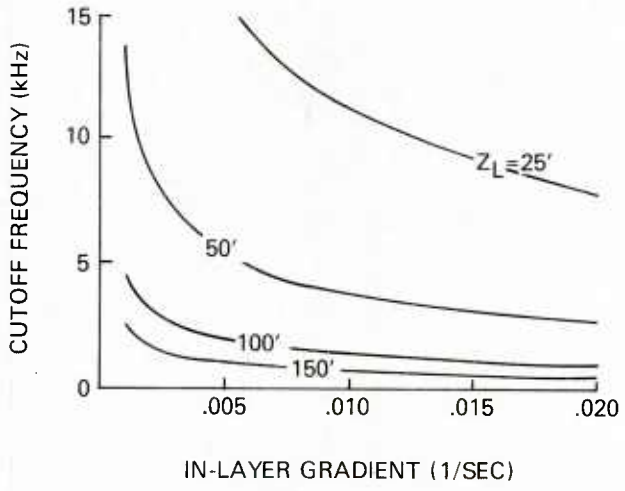

Figure 8. Cutoff frequency versus in-layer gradient

between 1 and 2. Using Eq. (18), the turning point depths for the first two modes are 2.32 H and 4.08 H, and hence for marginal trapping near cutoff

$$2.32 < M < 4.08. \tag{23}$$

This result indicates that the cutoff condition is approached for values of M as large as 4.

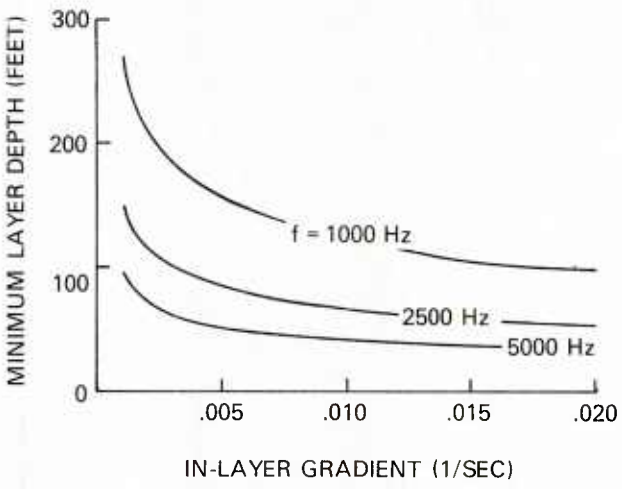

Figure 9. Minimum layer depth versus in-layer gradient

Some of the mode-parameter results presented here may appear to contradict the ray-parameter results of Sect. 2.3.1. What should be considered, however, is that the ray theory results merely provide guidance on how the channel-limiting cycle-range varies with in-layer gradient. These results say nothing about how acoustic energy is distributed throughout the channel. The mode parameters, however, provide guidance on how much energy is trapped in the duct as the in-layer gradient varies. Generally, as the in-layer gradient gets weaker less energy is trapped. Note also that none of the results presented here provides guidance on either cross-layer or below-layer performance. Such guidance is well beyond the capabilities of first-order WKB theory. Indeed, such guidance can be obtained only from mathematically more sophisticated threatments of the surface duct problem.

3.0 AMOS Models

The genesis of AMOS models began with a set of semiempirical equations derived from experimental data (Marsh and Schulkin, 1954). These equations are applicable to two near-surface propagation conditions, surface duct and subsurface duct. These conditions are handled by two distinct algorithms. Only the surface duct algorithm is addressed here. The original surface duct equations are partially reproduced in Appendix A. Models seldom survive for long without undergoing modifications in one form or another, and the AMOS model is no exception. Sections 3.1 through 3.3 address modifications that have been made to both NISSM and SHARPS III. Section 3.4 presents an assessment of the AMOS depth-loss functions.

3.1 Versions of AMOS

The AMOS model is modular in structure and is thus amenable to changes in specific components. The modifications that were made to the NISSM version of AMOS did not alter the basic range and depth-dependent functions. These modifications include changes in the expressions for the absorption coefficient and the surface scattering coefficient.

To extend the validity of the AMOS predictions to low frequencies an additive cutoff term has been incorporated. The cutoff term is based on an approximation to the normal-mode surface duct model of Pedersen and Gordon (1965). Details of the cutoff loss term are presented in Section 3.3.

Modifications to the SHARPS III version of AMOS are more dramatic than those applied to the NISSM version. Kirby (1981) refers to this version as Advanced AMOS. In Advanced AMOS the surface duct equations have been sensitized to both in- and below-layer velocity gradients. A rationale for this sensitization process is presented in Section 3.2.

3.2 A Gradient-Sensitive AMOS

The version of the AMOS surface duct equations presently used in SHARPS III has been modified to more properly reflect changes in propagation conditions that can result from slight changes in both in-layer and below-layer sound velocity gradients (Kirby, 1981). This modification, essentially, leaves the basic form of the depth-dependent factors unaffected, and hence the sensitivity to channel gradients still is not quite correct. Only the zone delineation parameters are affected. Reviewing the AMOS surface duct expressions (see Appendix A) they are seen to represent different spreading-law regimes depending on sonar-to-target separation range. Three such regimes are defined so that as range increases there is a "smooth" transition from spherical to cylindrical spreading. The quantities used in AMOS to define these transition ranges are referred to here as scaled zone-delineation parameters. These parameters are calculated from expressions having the forms

$$\rho(z) = (1 - t)/4, \text{ (in layer)} \quad (24)$$

and

$$\rho(z) = (t^2 - 1)^{1/2}/5, \text{ (below layer)} \quad (25)$$

where t^2 is the ratio of the sonar (or target) depth (Z) to the layer depth (Z_L). In the SHARPS version of AMOS, these expressions are replaced by similar quantities obtained from the continuous-gradient raytrace code that is used in other subroutines (Kirby, 1982). However, simple contant-gradient ray theory may be exploited to demonstrate how the channel gradients can be factored into the AMOS equations.

Essentially the quantities given in Eq. (24) and Eq. (25) represent scaled range segments along the channel-limiting ray that forms a circular trajectory connecting sonar and target. Each of the corresponding ray path segments takes the form

$$r_L(Z) = (C_L^2 - C_Z^2)^{1/2}/g, \quad (26)$$

where C_L and C_Z are the velocities at the layer depth and the sonar (or target) depth, respectively, and g is either the in-layer or the below-layer sound velocity gradient. This expression gives the horizontal range from a sonar (or target) depth to the point at the layer depth where the ray trajectory is horizontal. This expression can be approximated by

$$r_L(Z) = (2\bar{C}/g)^{1/2} (Z_L - Z)^{1/2} \quad (27)$$

where $\bar{C}$ is a nominal value of sound velocity. Let $\bar{C}$ = 4950 fps and let g take on the value 0.0176 fps/ft for the in-layer case and -0.0275 for the below-layer case. Then after converting from feet to kiloyards (dividing by 3000), the in-layer and below-layer segments are approximately

$$r_L(Z) = (Z_L - Z)^{1/2}/4, \text{ (in layer)} \quad (28)$$

and

$$r_L(Z) = (Z - Z_L)^{1/2}/5 \text{ (below layer)}. \quad (29)$$

Factoring out Z_L from the radicals yields

$$r_L(Z)/Z^{1/2} = (1 - t^2)^{1/2}/4 \text{ (in layer)} \quad (30)$$

and

$$r_L(Z)/Z_L^{1/2} = (t^2 - 1)^{1/2}/5 \text{ (below-layer)}. \quad (31)$$

Reducing the in-layer expression further to the form given in the original equations is difficult to rationalize, based on the simple assumptions made here. Nevertheless, replacing the original zone delineation expressions with expressions derived from constant-gradient ray theory is straightforward and appears to offer little risk with regard to altering other factors in the AMOS equations.

Of course, care must be exercised when the gradient-sensitive "skip" distance is factored into the AMOS equations. The original equations use scaled variables, where the scaling factor is twice the nominal skip distance. The so-called skip distance is the range spanned by the surface-to-surface channel limiting ray, given by

$$r_c = 2(C_L^2 - C_o^2)^{1/2}/g_o. \quad (32)$$

Advanced AMOS retains the nominal skip distance that is used in the original equations. Using the same values for C_o and g_o (in-layer value) as above, expressing the layer depth in feet, and converting to kiloyards yields

$$r_c \cong Z_L^{1/2}/2 \quad (33)$$

for the nominal skip distance (i.e, channel-limiting cycle range).

The following considerations indicate how a dependence on in-layer and below-layer gradients can be introduced into the AMOS equations (Appendix A) without at the same time introducing factors that might alter the depth-loss functions. A reasonable demarkation between the spherical spreading and transition zones is the range between sonar (Z_o) and target (Z) via the channel-limiting ray. Denoting this range by r_s, these zones are delineated by

$$r_s = r_L(Z_o) + r_L(Z). \quad (34)$$

If this equation is divided by $Z_L^{1/2}$, the scaled equivalent is approximately

$$\rho_s = \rho(Z_o) + \rho(Z). \quad (35)$$

A reasonable demarkation between the transition and cylindrical spreading zones is $r_s + r_c$. If these ranges are divided by $Z_L^{1/2}$, the scaled equivalent is given by $\rho_s + 1/2$, that is,

$$(r_s + r_c)/Z_L^{1/2} = \rho_s + 1/2. \quad (36)$$

Thus by simply replacing ρ_s by r_s and $\rho_s + 1/2$ by $r_s + r_c$, the AMOS equations become sensitized, partially at least, to the channel velocity gradients.

A similar treatment can be given to Eq. (A4) of Appendix A, although to do so requires some imagination along with a few gross assumptions. This equation can be rewritten as

$$H_A = 20 \log r + a_v r + (F/25)^{1/3} r_D,$$

where

$$r_D = 25 - (|Z_o - Z_L|)^{1/2} - (|Z - Z_L|)^{1/2} + 5r$$

or

$$r_D = 5[5 - (|Z_o - Z_L|)^{1/2}/5 - (|Z - Z_L|)^{1/2}/5 + r] \quad (37)$$

Now a "typical" layer depth is 100' so that a "typical" skip distance is 5 kyd ($=Z_L^{1/2}/2$). Thus the 5 that appears as the first term inside the brackets is replaced by r_c, the channel-limiting cycle range (or skip distance). The depth-dependent terms (very) approximately add up to r_s, the range between sonar and target via the channel limiting ray. Making these replacements yields,

$$r_D \cong 5[r_C - r_s + r]. \quad (38)$$

The particular approach taken here to introduce channel gradients into the

AMOS equations does not represent the only possibility. Other possibilities notwithstanding, however, the above gradient-sensitization scheme is used in demonstrating the impact of such a modification. An example of this gradient-sensitization process is illustrated in Figure 6. A comparison of Figure 5 and Figure 6 indicates that the variation with in-layer gradient agrees with ray theory. But, without also introducing gradient sensitivity into the depth-dependent factors, the sensitization as outlined here cannot be considered totally satisfactory. Additional comments on AMOS depth-dependence are presented in Section 3.4.

3.3 The Low Frequency Cutoff Term

One of the modifications made to the AMOS surface duct model when the NISSM model was developed is the addition of a low-frequency "cutoff" term. A review of the various NISSM and SHARPS documents reveals that explanations of the origin of this term are somewhat weak. The AMOS equations are semiempirical in nature, and as such do not exhibit features characteristic of mode solutions. The addition of the "cutoff" term is intended to partially account for mode attenuation effects. Since there is no mode-like summation in the AMOS model, the impact of an additive term should be minimal for conditions reflecting strong ducting. For conditions reflecting weak ducting, however, the addition of the first mode attenuation term should enhance the predictive ability of the AMOS model. Thus, the first-mode attenuation factor of a normal mode solution was decided upon.

The added term is referred to as a cutoff term because it is expected to have its major impact when only one trapped mode is present. That is, for any combination of frequency and profile parameters such that Eq. (19) yields a value of N near 1, the propagation of trapped energy is near cutoff. Holding the profile parameters constant, there is a minimum frequency that allows the duct to support one trapped mode. This cutoff frequency is given by Eq. (20).

The cutoff term used in NISSM is derived from the Pedersen and Gordon (1965) two-layer normal model surface duct mode. This model uses a rigorous normal mode solution to the wave equation. The solution can be written as

$$\Psi = -i\pi \sum_n H_o^{(2)}(k_n r) U_n(Z_o) U_n(Z) \qquad (39)$$

where the U_n are normalized eigenfunctions evaluated at source (Z_o) and receiver (Z) depths. If the Hankel function is replaced by the first term of its asymptotic expansion, propagation loss, H, can be expressed as

$$\begin{aligned} H &= -10 \log |\Psi^2| \\ &= -10 \log \left[\left(\sum A_n \cos\theta_n \right)^2 \right. \\ &\quad \left. + \left(\sum A_n \sin\theta_n \right)^2 \right] \\ &\quad -10 \log (C_o/f) + 10 \log r \end{aligned} \qquad (40)$$

where

$$A_n = U_n(Z_o) U_n(Z) \exp(-\tau_n r)$$

and

$$\theta_n = \arg[U_n(Z_o) U_n(Z)]. \qquad (41)$$

Note that this expression neglects effects due to surface reflection losses and volume absorption. To obtain Eq. (40) from Eq. (39) Pedersen and Gordon break down the separation parameter, k_n, as

$$k_n = k_o - \sigma_n - i\tau_n \qquad (42)$$

where generally k_o $(=2\pi f/C_o)$ is much greater than either σ_n or τ_n. In terms of the eigenvalues, MX_n, the separation parameter may also be expressed as

$$k_n = [k_o^2 - MX_n (M/Z_L)^2]^{1/2}$$
$$= k_o - (2k_o)^{-1} MX_n (M/Z_L)^2 \qquad (43)$$

Comparing Eqs. (42) and (43) yields the following expressions for σ_n and τ_n:

$$\sigma_n = (2k_o)^{-1} (M/Z_L)^2 Re(MX_n) \qquad (44)$$

and

$$\tau_n = (2k_o)^{-1} (M/Z_L)^2 Im(MX_n) \qquad (45)$$

If the channel strength parameter M is expressed in terms of frequency and profile parameters then the expression for τ_n can be written as

$$\tau_n = (\pi f g_o^2)^{1/3}/C_o \; Im(MX_n) \qquad (46)$$

Near cutoff Eq. (40) reduces to the single-mode expression

$$H = 10 \log r - 10 \log (C_o/f)$$
$$- 20 \log[|U_1(Z_o)U_1(Z)|]$$
$$- 20 \log[\exp(-\tau_1 r)] \qquad (47)$$

The first-mode attenuation term is the part that is appended to the AMOS surface duct equations. The remaining factors are assumed to be analogous to existing terms in the AMOS model. Thus the cutoff term takes the form

$$H_{CO} = -20 \log[\exp(-\tau_1 r)]$$
$$= 8.686 \; \tau_1 r \qquad (48)$$

The only remaining problem pertains to the imaginary part of the eigenvalues, $Im(MX_n)$. The calculations involved in detemining the MX_n are much too horrendous to be included in models like NISSM and especially SHARPS. A change in frequency or any of the profile parameters C_o, g_o, and Z_L results in a different set of eigenvalues. Thus to accommodate stringent computer-time requirements, a compromise must be made. Any given set of eigenvalues may be "indexed" by the parameter ρ, where

$$\rho^3 = -g_o/g_1$$

or

$$\rho = -(|g_o/g_1|)^{1/3} \qquad (49)$$

where g_o and g_1 are in-layer and below-layer sound velocity gradients. The possible combinations of g_o and g_1 are infinite, and hence there are as many possible choices of ρ. A value of -0.378 was selected for ρ. This value represents what the developers of the NISSM model felt was the most realistic compromise. Figure 10 illustrates selected curves of $IM(MX_n)$ versus the channel strength parameter M.

A slight improvement could be made to this approach by simply including additional curves corresponding to several values of ρ. In this way, all practical combinations of the gradients could be accommodated through interpolation.

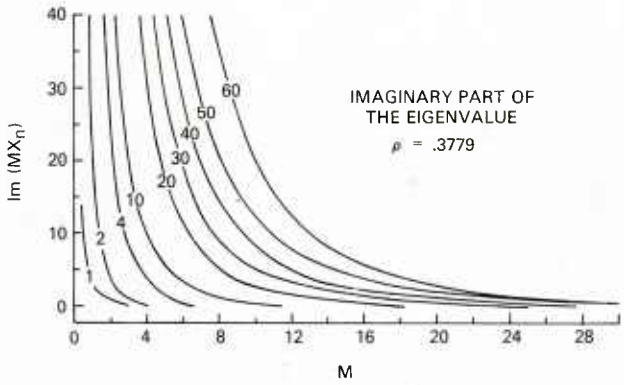

Figure 10. Imaginary part of eigenvalues versus M (from Watson and McGirr [1966]

3.4 Assessment of AMOS Depth Dependence

A major deficiency to look for in a simple model is its inability to represent the proper dependence of all important factors involved. Such a deficiency was discovered with the frequency dependence (for low frequencies) of the original AMOS model, and hence a low-frequency cutoff term was appended. In this section, the depth-dependence of the AMOS surface duct equations is examined. Depth-dependence is represented in these equations by two depth-loss functions. Actually these functions also involve frequency, but their sensitivity to sonar and target depths is the primary concern here. The first depth-loss function, denoted by $G(Z_o, Z)$, appears in Eqs. (A1) and (A2) (Appendix A). It takes the form

$$G(Z_o,Z) = (F/25)^{1/3} \begin{cases} 0.1 \times 10^{2.3|y_o - y|}, & |y_o - y| < 1 \\ 20, & |y_o - y| > 1, \end{cases} \quad (50)$$

where $F = f/1000$, $y_o = (Z_o/Z_L)^{1/2}$ and $y = (Z/Z_L)^{1/2}$. The variables Z_o and Z are sonar and target depths, respectively, and Z_L is the layer depth. The second depth-loss function, denoted by $K(Z_o, Z)$, appears in Eqs. (A2) and A3), and it takes the form

$$K(Z_o,Z) = [10^{y_o} + 10^{y} + 10^{|y-y_o|}] \begin{cases} 1, & F < 8 \text{ kHz} \\ (F/8)^{1/3}, & F > 8 \text{ kHz} \end{cases} \quad (51)$$

To isolate the effects of these two functions, the depth-dependence of Eqs. (A1), (A2), and (A3) are examined at three ranges. The effects of the function $G(Z_o, Z)$ can be isolated by selecting a value of range, r, such that $r < r_s$. Referring to Eq. (49), r_s is seen to be the maximum range for which Eq. (A1) applies. Similarly the effects of $K(Z_o, Z)$ can be isolated by selecting a value of range such that $r > r_s + r_c$. Referring to Eq. (47), $r_s + r_c$ is seen to be the minimum range for which Eq. (A3) applies. The effects of G and K in combination can be examined by selecting a value of r that lies midway between r_s and $r_s + r_c$.

As a control to compare against, simple WKB solutions are evaluated as a function of depth at the same ranges. The normalized eigenfunctions are given by Eqs. (9a) and (9b). For cases that yield a sufficient number of strongly trapped modes, WKB solutions yield reasonable results except when evaluated too close to turning point depths. However, since the assessment here is restricted to in-layer geometries, interpolation of the $U_n(Z)$ between points on either side of turning point depths yields results that are reasonably close to their normal mode counterparts.

The expression for mode attenuation is

$$\alpha_n = -10 \log[\exp(-2b_n)]$$

(see for example Kibblewhite and Denham, (1965). In this expression the mode dependent factor b_n is given by

$$b_n = -\mathrm{Im}(k_n)/(2K_n)$$

$$= (2D_n)^{-1} \exp[-(4/3)k_o\beta_o^{1/2}$$

$$(1 + \beta_0/\beta_1)(Z_L - Z_n)^{3/2}] \qquad (52)$$

where $\beta_o = 2g_o/C_o$, $\beta_1 = -2g_1/C_o$ and Z_n is the upper turning point depth of the n-th "mode". The quantity D_n is the cycle distance of mode n, and can be expressed in terms of the range integral of Eq. (3) evaluated from the surface to the turning point depth, Z_n. Using Eq. (52) to calculate "modal" attenuations and neglecting volume attenuation and surface reflections, the WKB expression for in-layer incoherent propagation loss, H_w, is

$$H_w = 10 \log(2\pi) + 10 \log r$$

$$- 10 \log\left(\sum_n P_n^2\right) \qquad (53)$$

where

$$P_n = U_n(Z_o)\, U_n(Z) \exp(-b_n r).$$

The depth-dependence of Eq. (53) is compared to the appropriate AMOS equation. The particular AMOS equation to be compared against depends on the applicable range regime. Shed of volume attenuation and surface reflection loss terms, the AMOS equations reduce to:

for $r < r_s$ (spherical spreading zone)

$$H_A = 20 \log r + (r/r_s)\, G(Z_o, Z), \qquad (54)$$

for $r_s < r < r_s + r_c$ (transition zone)

$$H_A = 20 \log r + (1 - \delta)\, G(Z_o, Z)$$

$$+ \delta K(Z_o, Z) + H_{co} \qquad (55)$$

where

$$\delta = (r - r_s)/r_c$$

and for $r > r_s + r_c$ (cylindrical spreading zone)

$$H_A = 10 \log r + 10 \log(r_s + r_c)$$

$$+ K(Z_o, Z) + H_{co}. \qquad (56)$$

Figure 11 illustrates propagation loss versus depth evaluated (from left) at ranges of 4, 8, and 12 kyd. AMOS and WKB results are presented for a frequency of 2.5 kHz, a source depth of 20 ft and with receiver depth varying in one-foot increments from the surface

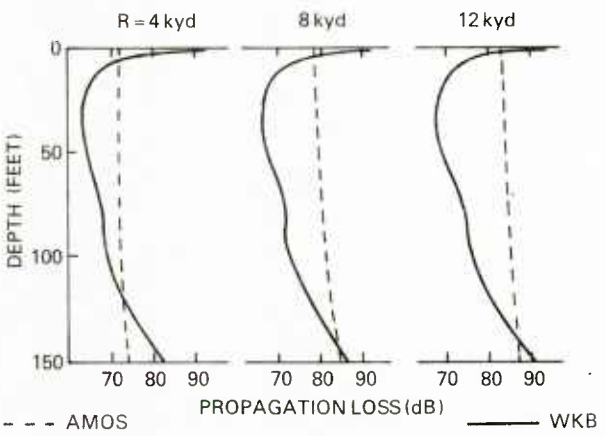

Figure 11. Comparison of AMOS and WKB depth dependence

down to the layer depth. The sound velocity at the surface is 4950 ft/sec, the layer depth is 150 ft, and the in-layer and below-layer velocity gradients are 0.02 and -0.33 1/sec, respectively. The dashed, nearly straight curves represent the AMOS results. The WKB results, indicated by the solid curves, exhibit far more depth-dependence than their AMOS counterparts. Indeed, the AMOS curves demonstrate extremely scant variation with depth. A slight slope is barely perceptible in the AMOS curves, and they are essentially constant with depth. Their most significant departure from what is expected is disclosed by the finite value at the surface. The WKB solutions are subject to the requirement of zero pressure at the surface, and hence the loss evaluated there is infinite. Actually this particular discrepancy of the AMOS model is not a serious drawback as far as SHARPS applications are concerned, since most sonars and targets of interest are situated at depths of at least 20 ft or more.

A more serious deficiency is the lack of any "mode-like" dependence on channel gradients. As the in-layer gradient decreases, the number of trapped modes likewise decreases. There is no way to account for this behavior in the AMOS surface duct model. the gradient-sensitized zone delineation parameters exhibit the correct variation, but the depth-dependent factors do not properly compensate for off-setting mechanisms such as modal excitation or leakage.

4.0 Near-Surface Propagation Modeling

Many of the sound velocity profile configurations discussed in Section 2 exhibit substantial departure from the idealized two-layer surface duct model. Indeed, the variation in profile configurations suggests that the AMOS model and perhaps other candidate near-surface models are unable to meet Fleet prediction requirements. This section reviews long-standing near-surface channel issues, and presents results of a recent evaluation of three operational surface duct models.

4.1 A Review of Near-Surface Channel Issues

Results reported by both Morris (1974) and Hall (1980) indicate that, when compared to experimental surface duct data, the AMOS model does about as well, on average, as more sophisticated normal mode models. This conclusion should not be interpreted to mean that the AMOS model is as accurate as normal mode theory. As Hall also notes, on a case-by-case basis normal mode theory does a better job than the AMOS model. Unfortunately, as discussed in Section 2, the configuration of a surface duct does not sustain itself over either long durations or long ranges. Indeed, the channel above the sonic layer depth can conform to a wide variety of configurations. The point is, even if the AMOS model does an acceptable job of predicting surface duct propagation loss, at least on average, it cannot handle several other important near-surface channel configurations.

The following issues are pertinent to SHARPS and perhaps to other operational prediction models as well.

1. isovelocity and weak-gradient channels
2. the afternoon effect
3. non-symmetric depressed ducts
4. multiple duct coupling
5. coupling of rough surface effects

No attempt is made here to prioritize these issues. Most of them are long-standing issues, and they are all important.

Isovelocity and weak-gradient channels can probably be modeled, at least as an interim measure, by the surface duct equations of Advanced AMOS. Computational problems caused by zero gradients can be avoided by limiting the

gradient to some arbitrary lower bound, say 0.005 1/sec. Such an ad hoc procedure creates a bit of consternation, however, since the depth-dependent functions used in AMOS are based on data collected under conditions of energy trapping. Without the requisite energy barrier present, the AMOS depth-loss functions no doubt give erroneous results.

The afternoon-effect profile is very similar to the classical surface duct profile except for the upper few meters where there is a (sometimes sharp) negative gradient. Its occurrence may be more prevalent than indicated by the SUDS I statistics (Sect. 2.2). The presence of such configurations is elusive to measurement programs, owing to their transient nature. Properly accounting for the negative gradient in the upper few meters can be crucial in modeling the detection performance of hull-mounted sonars. Unless some "rule of thumb" can be appended to the AMOS model to properly modify its subsurface duct predictions, a three-layer propagation model is probably required. The subsurface duct equations of AMOS are not appropriate without modifications, since they require a profile configuration that is (nearly) symmetrical.

A related problem is one posed by non-symmetric depressed channels in general. Such profiles tend to present a modeling problem because, typically, their gradients are weak and hence leaky modes become important contributions to propagation loss calculations. Approximate methods (e.g., WKB-inspired solutions) yield elusive computational adventures at best. Even precise normal mode codes run into numerical problems in attempts at finding eigenvalues for profiles replete with weak gradients (Pedersen and McGirr, 1982).

The multiple duct coupling problem is especially crucial to modeling the detection performance of variable depth sonars and tactical towed arrays. A receiver positioned within a subsurface duct could, under the right conditions, pick up signals generated by a target positioned in an overlying surface duct. However, the current version of AMOS used in the SHARPS model cannot simulate this type of coupling phenomenon.

The coupling of rough surface effects is probably a moot point as long as the AMOS model is retained as the SHARPS near-surface propagation model. If, on the other hand, a decision is made to replace AMOS with a more sophisticated normal mode (or mode-like) model, then this issue is pertinent. Barnard and Deavenport (1976) have demonstrated how WKB techniques can be exploited to enhance predictions generated by the Pedersen and Gordon surface duct model. Bucker (1980) uses a mode-coupling scheme to fully integrate surface scattering into the mode solution. Results obtained by using various coupling schemes are in dramatic contrast with results obtained by using a simple add-on approach.

The issue of confidence bounds has been around long enough to have disappeared from the list of issues. But it is still an issue. The idea of generating a detection range interval vice a particular range makes a lot of sense, especially for prediction models like SHARPS. Forecasts intended to cover a specified time period cannot reliably predict instantaneous results based on data derived from a long string of averages supplemented by archived data. Although all terms of the sonar equation are affected by fluctation phenomena, the development of a simple scheme to estimate a confidence envelope for propagation loss predictions would go a long way toward solving the total problem.

4.2 Operational Surface Duct Propagation Models

This section presents highlights from a recent review of three operational propagation loss models, with comments

restricted to their performance in predicting surface duct loss. At the outset some clarification of what passes as an operational model is in order. The significance of the term operational is somewhat elusive, and no attempt is made here to be precise in the matter. Certainly any model that is routinely used in support of Fleet operations can be considered an operational model. On less solid grounds are those models that are excluded from the Fleet support category but are relatively user friendly and enjoy wide usage throughout the ASW R&D community.

The three models of interest here are FACT, FAME, and RAYMODE. FACT (Fast Asymptotic Coherent Transmission) and RAYMODE have been widely used throughout the ASW R&D community for more than 10 years. Moreover, both of these models (or derivatives therefrom) are being used as components of operational performance prediction models. They have been subjected to minor modifications from time to time, and both are presently under configuration management control (CMC). FAME (Fast Multipath Expansion) is a relatively new model and is not yet under CMC.

The mathematics and physics behind each of these models are presented in various documents. FACT uses modified ray theory to calculate propagation loss via bottom reflected and RSR paths. To the most recent verison, special modules based on normal mode theory have been added to calculate propagation loss for surface ducts and half channels. The modified ray theory used in the original version of FACT is documented in a report by Spofford (1974). Except for improvements to the caustic correction algorithms, this documentation is still applicable for bottom reflected and RSR paths. Improvements to the treatment of caustics are documented in a report by Spofford, et al. (1977). The surface duct and half channel modules are documented by Ryan (1980, 1982). The multipath expansion (MPE) method is described in an article by Weinberg (1975). Additional remarks can also be found in a report documenting the Generic Sonar Model (GSM) (Weinberg, 1979). Documentation of the RAYMODE model has always been difficult to get. However, some hard-to-get documents that are helpful in understanding the model physics are the reports by Leibiger (1968 and 1971). Other documents pertinent to the physics of FACT and RAYMODE are the evaluation reports by Bartberger (1978b, 1981) and Deavenport (1978). An excellent summary of propagation modeling in general, which also includes discussions pertaining to both the multipath expansion method and the RAYMODE method, is presented by Di-Napoli and Deavenport (1979).

Both FACT and RAYMODE have special "stand-alone" modules for calculating surface duct propagation loss. FAME does not, however, and hence comparing the times that these models spend on surface duct calculations presents a problem. Out of deference to the FAME model, Keenan (1983) presents computation times that include bottom reflected paths as well. Keenan compares computation times for ten environments. For each of these, the source depth is at 50 ft and computation times for separate model runs are presented for two receiver depths, 50 ft and 300 ft, and for three frequencies, 500, 1000, and 4000 Hz. Mean computation times derived from these ten cases indicate that FACT is roughly twice as fast as RAYMODE and at least an order of magnitude faster than FAME.

Keenan (1983) takes two approaches in evaluating the accuracy of these models. In one approach, the three models are evaluated strictly on a comparative basis (a PE model was also exercised against the same inputs but unfortunately these results are not included). In a second approach, the models are compared to data measured during the SUDS I experiment. Conclusions are difficult to draw from the strictly comparative results. Keenan presents curves generated by these

models in typical overlay fashion. Both coherent and incoherent results are presented. Normally, incoherently summed propagation loss calculations yield curves that exhibit a fairly smooth variation with range, except of course in regions like convergence zones where a certain amount of multipath beat-structure is typically evident.

For most of the cases presented, both FAME and RAYMODE exhibit (but not consistently) saw-tooth structure in their incoherent results. The reason for such unexpected coherent-like structure is not at all clear, but its presence makes comparative analyses nearly impossible. For those cases where the RAYMODE incoherent outputs are fairly smooth there is good agreement between FACT and RAYMODE. For those cases where the RAYMODE incoherent outputs are choppy there appears to be good agreement between FAME and RAYMODE.

Comparisons againt SUDS data are presented for two frequencies, 400 and 1000 Hz, and several combinations of source and receiver depths. At 400 Hz RAYMODE is consistently close to the experimental data, whereas FAME is far too optimistic and FACT is far too pessimistic. At 1000 Hz the comparisons are inconsistent, although FACT appears to hang with the data closer than the other two models, especially at ranges exceeding about 10 km. FACT appears to be the most accurate of the three at the higher frequency. It is certainly the fastest, and, therefore, it may also be worth considering as a replacement for the AMOS model.

5.0 Conclusions and Recommendations

The near-surface channel configurations addressed by the current version of SHARPS are too limited. The options are limited to surface ducts and subsurface ducts, as modeled by the Advanced AMOS equations. All other channel configurations are handled by ray theory. The omission of a mechanism to account for cross-duct coupling is a glaring deficiency, especially in view of the latitude in depth available to modern submarines. Criticizing a model as vulnerable as SHARPS is easy. What is not so easy is how to reconcile deficiencies without introducing computer code that consumes an excessive number of CPU seconds.

The options addressed here are placed into three levels. These levels correspond to two extremes and a compromise. One extreme is dictated by severe computer-time constraints imposed on models that are used in generating daily forecasts at FNOC. The other extreme allows for solutions to be formulated with no considerations given to computer time-storage constraints. Midway between these extremes lies a set of compromise solutions that, in turn, are contingent on a slight relaxation of current computer-time constraints.

LEVEL I: Under presently imposed computer-time constraints, virtually no additional computing time can be consumed by modifications to SHARPS. This criterion effectively limits improvements to those that might enhance the existing surface duct and subsurface duct models (e.g., more modifications to AMOS). There are two modifications that could yield improvements from the AMOS model. One modification entails deriving new depth-loss functions from normal mode theory. Actually, this approach has already been applied and the results have been used to complement the ray theory calculations in PLRAY (Bartberger, 1978a). The advantage of this approach is that the resulting depth-dependent functions would exhibit a more realistic sensitivity to in-layer and below-layer sound velocity gradients.

A second modification entails appending an energy-barrier transmission coefficient to simulate surface duct to subsurface duct coupling. That is, the amount of energy that tunnels through the barrier separating the ducts could

be approximated by a WKB transmission coefficient. This coefficient is obtained by integrating over the vertical wave number from a turning point depth in the surface duct to a conjugate turning point depth in the subsurface duct. Since AMOS does not sum over modes, only one pair of turning points would be appropriate. This approach is strictly ad hoc in nature, and constitutes pushing the applicability of the time-worn AMOS model well-beyond its intended limits.

LEVEL II: A number of options open up at this intermediate level. The easing of computer-time constraints that would be necessary is not quantifiable at this conceptual stage. No doubt some slight adjustments would have to be made to the present forecasting schedule.

At this level most of the current near-surface modeling deficiencies could be eliminated. Ryan (1983) has indicated that phase integral methods could be exploited to develop an approximate, four-layer normal mode model. Thus most of the near-surface channel configurations discussed in Sect. 2 could be modeled. Moreover, cross-duct coupling could be modeled using WKB techniques.

LEVEL III: The prerequisite for considering level-III options is a significant upgrade in computing power. With adequate computing facilities a high-volume load could be accommodated without having to make sacrifices in model physics. Indeed, a multi-layer normal mode treatment could be applied to all modes of propagation, complete with mode coupling to account for both forward- and back-scattering effects.

6.0 References

Anderson, E. R. and M. A. Pedersen (1976). Surface-Duct Sonar Measurements (SUDS I - 1972) Technical Report. NUC TP 463, November.

Barnard, G. R. and R. L. Deavenport (1978). Propagation of Sound in Underwater Surface Channels with Rough Boundaries. J. Acoust. Soc. Am., 63: 709-714.

Bartberger, C. L. (1978a). PLRAY--A Ray Propagation Loss Program. NADC Report 77296-30, 26 October.

Bartberger, C. L. (1978b). The Physics of the FACT Model. Encl (1) to NUSC/NL ltr ser 9312-55, 19 December.

Bartberger, C. L. (1981). An Investigation of the Physics of the RAYMODE Model. NADC Report 82009-30, 24 November.

Bucker, H. P. (1980). Wave Propagation in a Duct with Boundary Scattering (with Application to a Surface Duct). J. Acoust. Soc. Am., 68:1768-1772, December.

Deavenport, R. L. (1978). RAYMODE Physics Evaluation. Encl (2) to NUSC/NL ltr ser 9312-55, 19 December.

DiNapoli, F. R. and R. L. Deavenport (1979). Numerical Models of Underwater Acoustic Propagation. Chapter 3 in Ocean Acoustics, ed. by J. A. DeSanto, Springer-Verlag.

Freehafer, J. E. (1951). Phase-Integral Methods. Sect. 2.8, and The Field Integral. Sect. 2.10 in Propagation of Short Radio Waves, ed. by D. E. Kerr, McGraw-Hill.

Furry, W. H. (1945). Theory of Characteristic Functions in Problems of Anomalous Propagation. MIT Lab Rept 680.

Hall, M. (1976). Mode Theory of Wave Propagation in a Bilinear Medium: The WKB Approximation. J. Acoust. Soc. Am., 60:810-814.

Hall, M. (1980). Surface Duct Propagation: An Evaluation of Models of the

Effects of Surface Roughness. J. Acoust. Soc. Am. 67:803-811.

Keenan, R. E. (1983). Final Report Volume IV: SUBCOM, FAME, RAYMODE and FACT Comparisons of Accuracy and a Computation Time in a Surface Duct Environment. SAI-84-153-WA, April.

Kibblewhite, A. C. and R. N. Denham (1965). Experiment on Propagation in Surface Sound Channels. J. Acoust. Soc. Amer. 38:63-71.

Kirby, W. D. (1981). Program Specification for AMOS Module Within SHARPS III. SAI-82-566-WA, August.

Kirby, W. D. (1982). Technical Description for the Ship Helicopter Acoustic Range Prediction System (SHARPS III). SAI-83-1071, December.

Leibiger, G. A. (1968). Application of Normal Mode Theory to Propagation of 3.5 kHz Pulses in Shallow Water. VL-2476-9-0, 25 June.

Leibiger, G. A. (1971). A Combined Ray Theory-Normal Mode Approach to Long Range, Low Frequency Propagation Loss Prediction (U). NUSC Tech Memo PA3-0109-71, 13 August.

Marsh, H. W. and M. Schulkin (1954). Report on the Status of Project AMOS (Acoustic, Meteorological, and Oceanographic Survey). USNUSL Report 255A.

Morris. H. C. (1974). Comparison of Propagation Prediction Models with SUDS I Acoustic Data. NUC TP 377, April.

Pedersen, M. A. and D. F. Gordon (1965). Normal Mode Theory Applied to Short-Range Propagation in an Underwater Acoustic Surface Duct. J. Acoust. Soc. Am., 37:105-118.

Pedersen, M. A. and R. W. McGirr (1982). Use of Theoretical Controls in Underwater Acoustic Model Evaluation. NOSC TR 758, 4 January.

Renner, W. W. and W. D. Kirby (1983). Sound Velocity Profile Filter Evaluation. SAI-84-227-WA, August.

Ryan, F. J. (1980). Virtual Mode Surface Duct Model for FACT. SAI-81-259-WA, September 28.

Ryan, F. J. (1982). Phase Integral Methods. Unpublished notes.

Ryan, F. J. (1983). FACT 81B Software Functional Description. SAI-011-82-270-LJ, October 13.

Spofford, C. W. (1974). The FACT Model. Vol. I, (AESD) MC Report 109, November.

Spofford, C. W., R. E. Keenan, and W. W. Renner (1977). Implementation of Rough Surface, Surface Duct, and Cusped Caustic Improvements in FACT. SAI-78-688-WA.

Watson, W. H. and R. W. McGirr (1966). A Surface Channel Propagation Loss Model I. NE1 TM 921, 30 March.

Weinburg, H. (1975). Application of Ray Theory to Acoustic Propagation in Horizontally Stratified Oceans. J. Acoust. Soc. Am., 58:97-109, July.

Weinberg, H. (1979). Generic Sonar Model. NUSC TD 5971, 1 January.

Appendix: AMOS Surface Duct Model

The purpose of this appendix is to present the basic (pre-NISSM) AMOS surface duct equations. Expressions for volume absorption and surface reflection loss are omitted. Essentially there are four propagation loss equations. Three of these give propagation loss corresponding to spreading-law regimes. The fourth equation provides an upper bound (on the loss) to the other three. With Z_o and Z denoting, respectively, source depth and receiver depth, AMOS propagation loss H_A, is given by

$$H_A = 20 \log r + \alpha_v r + (\rho/\rho_s)\, G(Z_o,Z) \qquad (A1)$$

$$H_A = 20 \log r + \alpha_v r + (1 - d)\, G(Z_o,Z) + d\, K(Z_o,Z) \qquad (A2)$$

where

$$d = 2(\rho-\rho_s)$$

$$H_A = 10 \log r + \alpha_v r + K(Z_o,Z) + [r - Z_L^{1/2}(\rho_s + 1/2)]\alpha_s + 10 \log [Z_L^{1/2}(\rho_s + 1/2)] \qquad (A3)$$

$$H_A = 20 \log r + \alpha_v r + [25 - (Z_o - Z_L)^{1/2} - (Z - Z_L)^{1/2} + 5r]\, (F/25)^{1/3} \qquad (A4)$$

where F=f/1000 and the depth-loss functions G and K are given by Eqs. (50) and (51). The scaled parameters ρ and ρ_s are discussed in Section 3.2. Surface roughness effects and column absorption losses are represented by the attenuation coefficients α_s and α_v. Eq. (A1) is essentially a spherical-spreading law with an additional depth-loss function, $G(Z_o,Z)$. Eq. (A3) is essentially a cylindrical-spreading law with an additional depth-loss function, $K(Z_o,Z)$. Eq. (A2) provides a smooth transition from spherical spreading to cylindrical spreading. Eq. (A4) provides an upper bound on propagation loss. This last equation is always compared with whichever of the other three is applicable and the smallest value is used for the final result. The spreading-law zones are delineated by using the scaled parameters ρ_s and $\rho_s + 1/2$.

Spherical spreading: $\rho < \rho_s$
Eq. (A1) applies

Transition zone: $\rho_s < \rho < \rho_s + 1/2$
Eq. (A2) applies

Cylindrical spreading: $\rho > \rho_s + 1/2$
Eq. (A3) applies

Distribution List

Department of the Navy
Asst Deputy Chief of Navy Materials
for Laboratory Management
Rm 1062 Crystal Plaza Bldg 5
Washington DC 20360

Department of the Navy
Asst Secretary of the Navy
(Research Engineering & System)
Washington DC 20350

Project Manager
ASW Systems Project (PM-4)
Department of the Navy
Washington DC 20360

Department of the Navy
Chief of Naval Material
Washington DC 20360

Department of the Navy
Chief of Naval Operations
ATTN: OP 951
Washington DC 20350

Department of the Navy
Chief of Naval Operations
ATTN: OP 952
Washington DC 20350

Department of the Navy
Chief of Naval Operations
ATTN: OP 987
Washington DC 20350

Director
Chief of Naval Research
ONR Code 420
Ocean Science & Technology Det
NSTL, MS 39529

Director
Defense Technical Info Cen
Cameron Station
Alexandria VA 22314

Commander
DW Taylor Naval Ship R&D Cen
Bethesda MD 20084

Commanding Officer
Fleet Numerical Ocean Cen
Monterey CA 93940

Director
Korean Ocean R&D Inst
ATTN: K. S. Song, Librarian
P. O. Box 17 Yang Jae
Seoul South Korea

Commander
Naval Air Development Center
Warminster PA 18974

Commander
Naval Air Systems Command
Headquarters
Washington DC 20361

Commanding Officer
Naval Coastal Systems Center
Panama City FL 32407

Commander
Naval Electronic Sys Com
Headquarters
Washington DC 20360

Commanding Officer
Naval Environmental Prediction
Research Facility
Monterey CA 93940

Commander
Naval Facilities Eng Command
Headquarters
200 Stovall St.
Alexandria VA 22332

Commanding Officer
Naval Ocean R & D Activity
ATTN: Codes 110/111
Code 125
Code 200
Code 300
Code 115
Code 500
NSTL MS 39529

Director
Liaison Office
Naval Ocean R & D Activity
800 N. Quincy Street
502 Ballston Tower #1
Arlington VA 22217

Commander
Naval Ocean Systems Center
San Diego CA 92152

Commanding Officer
Naval Oceanographic Office
NSTL MS 39522

Commander
Naval Oceanography Command
NSTL MS 39522

Superintendent
Naval Postgraduate School
Monterey CA 93940

Commanding Officer
Naval Research Laboratory
Washington DC 20375

Commander
Naval Sea System Command
Headquarters
Washington DC 20362

Commander
Naval Surface Weapons Center
Dahlgren VA 22448

Commanding Officer
Naval Underwater Systems Center
ATTN: New London Lab
Newport RI 02840

Director
New Zealand Oceano Inst
ATTN: Library
P. O. Box 12-346
WELLINGTON N., NEW ZEALAND

Director
Office of Naval Research
Ocean Science & Technology Div
NSTL MS 39529

Department of the Navy
Office of Naval Research
ATTN: Code 102
800 N. Quincy St.
Arlington VA 22217

Commanding Officer
ONR Branch Office
536 S Clark Street
Chicago IL 60605

Commanding Officer
ONR Branch Office LONDON
Box 39
FPO New York 09510

Commanding Officer
ONR Western Regional Ofs
1030 E. Green Street
Pasadena CA 91106

President
Texas A&M
ATTN: Dept of Ocean Working Collection
College Station TX 77843

Director
University of California
Scripps Institute of Oceanography
P. O. Box 6049
San Diego Ca 92106

Director
Woods Hole Oceanographic Inst
Woods Hole MA 02543